CHEMISTRY OF MATERIALS
Article
Cite This: Chem. Mater. 2019, 31, 216−223
pubs.acs.org/cm

Synthesis of $(BiSe)_{1+\delta}(Bi_2Se_3)_{1+\gamma}(BiSe)_{1+\delta}TiSe_2$ by Directed Self-Assembly of a Designed Precursor

Alexander C. Lygo, Suzannah R. Wood,[†] Jeffrey Ditto, and David C. Johnson*

Department of Chemistry, Materials Science Institute, University of Oregon, Eugene, Oregon 97403, United States

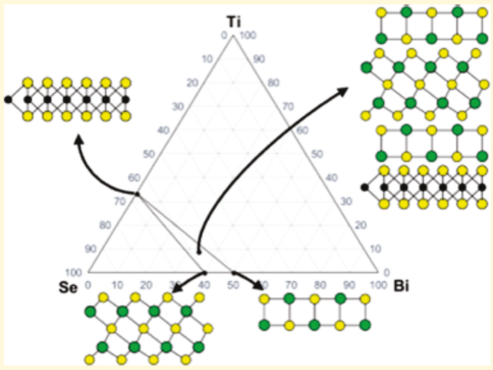

ABSTRACT: The synthesis, structure, and properties of a new three-constituent heterostructure containing BiSe, Bi_2Se_3, and $TiSe_2$ layers, each with a different structural motif, are reported. $(BiSe)_{1+\delta}(Bi_2Se_3)_{1+\gamma}(BiSe)_{1+\delta}TiSe_2$, where δ and γ are the misfit parameters representing the differences in the in-plane packing density of the constituents, forms via a self-assembly process during low-temperature annealing from precursors with a range of compositions and repeat period thicknesses. This indicates that the compound exists in a relatively broad and deep free-energy minima in the energy landscape. The formation was followed as a function of annealing temperature using X-ray diffraction to determine optimum annealing temperatures and stability range. High-resolution electron microscopy images revealed the layering sequence of the constituents and a supercell within the BiSe layers created by periodic anti-phase boundaries. Temperature-dependent electrical transport measurements show unexpected changes in carrier mobility and concentration relative to $(BiSe)_{1.15}TiSe_2$. This study suggests that new ternary and multinary phases containing fragments of known binary phases can be synthesized via precursors that mimic the desired product and that the properties of these new phases with ultrathin constituent thicknesses will probably be different from that expected based on composite behavior.

The synthesis of new solid-state compounds with targeted structures and/or desired properties has historically been challenging because traditional synthesis techniques typically yield the thermodynamic products and the desired compounds are often metastable. Recently, the discovery of topological materials with potential applications in high-performance electronics and quantum computers[1−4] has resulted in a search for new materials with both enhanced and new topological properties. A common approach for discovering new topological materials is to incorporate structural units of known topological compounds into heterostructures.[5−7] The van der Waals gaps on either side of the Se−Bi−Se−Bi−Se layers in Bi_2Se_3 and the fact that Bi_2Se_3 is an extensively studied topological insulator with a robust single Dirac cone, thickness-dependent band structure, and defect-induced band bending[8−10] make it a particularly attractive structural unit.[11] Unfortunately, different layer by layer growth conditions required for each constituent often prevent the synthesis of targeted heterostructures via epitaxial approaches.[12]

Our approach to this challenge is to prepare precursors with composition profiles that mimic the desired product. Elemental layers are deposited on room-temperature substrates, which are annealed at low temperatures to self-assemble the targeted products while limiting diffusion and preserving the as-deposited (AD) architecture. In a prior study, we deposited repeating structures with the layer sequence $(Bi|Se)_n(Ti|Se)_n$ where n = 2 and 3 to explore the existence of a potential new heterostructure containing bilayers or trilayers of both BiSe and $TiSe_2$ in the unit cell.[13] On heating, several precursors crystallized into a heterostructure with a c-axis lattice parameter of ~27.5 Å with varying degrees of structural coherence.[14] The observation of a superlattice with a c-axis lattice parameter of ~27.5(1) Å forming over a range of composition suggested that the compound forming must exist in a broad and relatively deep local free energy minimum in the free energy landscape relative to alternative compounds with a similar composition.[14−17]

This paper explores the synthesis, structure, and properties of this unknown compound. The reported composition and c-axis lattice parameter of ~27.5(1) Å is consistent with a compound that comprises one quintuple layer of Bi_2Se_3 (c = ~9.5 Å), two bilayers of BiSe (c = ~6 Å), and one layer of $TiSe_2$ (c = ~6 Å). Using the stoichiometry of previously reported $BiSe_{1.15}TiSe_2$ and the a-lattice parameter of Bi_2Se_3, the expected composition of a compound with layers of BiSe separating Bi_2Se_3 and $TiSe_2$ layers is 33.44% Bi, 57.70% Se, and 8.86% Ti.[17,18] In this study, we prepared precursors with composition and periods near that expected for the compound $(BiSe)_{1+\delta}(Bi_2Se_3)_{1+\gamma}(BiSe)_{1+\delta}TiSe_2$, and each formed this compound with secondary phases consistent with deviations from the targeted composition. The compound $(BiSe)_{1+\delta}(Bi_2Se_3)_{1+\gamma}(BiSe)_{1+\delta}TiSe_2$ began to self-assemble during the deposition and fully formed after annealing at 350 °C. Annealing at higher temperatures resulted in decomposition to

Received: October 4, 2018
Revised: December 5, 2018
Published: December 6, 2018

DOI: 10.1021/acs.chemmater.8b04229
Chem. Mater. 2019, 31, 216−223

amorphous TiO_2 and Bi_2Se_3 because of reaction with oxygen. The structure was determined via Rietveld refinement, using atomic plane positions determined from high-angle annular dark field scanning transmission electron microscopy (HAADF-STEM) images as a starting model. The structures of the constituent layers were consistent with the respective binary compounds. The HAADF-STEM images revealed extensive rotational disorder of the constituent layers. Electrical transport properties were different from those expected based on a simple composite behavior of the constituents, presumably because of interactions between the layers.

EXPERIMENTAL METHODS

The compound $(BiSe)_{1+\delta}(Bi_2Se_3)_{1+\gamma}(BiSe)_{1+\delta}TiSe_2$ was synthesized using the modulated elemental reactants technique.[19] Precursors were prepared by sequentially evaporating elemental sources of Bi, Ti, and Se on (100) oriented Si wafers in the specific sequence (Bi|Se)(Bi′|Se′)(Bi|Se)(Ti|Se) to kinetically trap the targeted compound. The compositions and thicknesses of the Bi|Se and Ti|Se bilayers were those used previously to form the compound $(BiSe)_{1.15}TiSe_2$.[17] The thickness and composition of the Bi′|Se′ layer was adjusted such that each precursor bilayer formed a single Se−Bi−Se−Bi−Se layer as found in Bi_2Se_3. Precursors were annealed at various temperatures in a N_2 glovebox with a concentration of oxygen below 0.6 ppm to induce diffusion and self-assembly of the targeted product.

Specular X-ray diffraction (XRD) was performed to determine the degree of order perpendicular to the substrate on a Bruker D8 DISCOVER diffractometer equipped with Cu Kα radiation (λ = 0.15418 nm), Göbel mirrors, and Bragg−Brentano θ−2θ optics geometry. In-plane XRD was done on a Rigaku SmartLab diffractometer equipped with Cu Kα radiation. The repeat thicknesses and c-axis lattice parameters were calculated using modified Braggs' law. Out-of-plane Rietveld refinement and in-plane full pattern Le Bail fits were done in the FullProf software suite.[20−22]

Compositional analysis was conducted using X-ray fluorescence spectroscopy collected using a Rigaku ZSX Primus II wavelength-dispersive X-ray fluorescence spectrometer with a rhodium X-ray source. Intensity was measured by integrating the area under the entire peak measured in intensity as a function of 2θ using MATLAB's cubic smoothing spline function with the smoothing parameter set to zero smoothing. Data were also collected for substrates without any deposited film. The intensity data measured for the clean substrates were treated in the same manner as the deposited samples. The resulting integrated counts of the clean substrate were subtracted from the integrated intensity of the coated substrates to correct for the background signal and any signal from the substrate itself. The proportionality constant between the X-ray fluorescence (XRF) intensity and the atom density per unit area for each element was determined as described previously.[23]

Samples were prepared for HAADF-STEM on a FEI Helios 600 dual-beam using a technique described by Schaffer et al.[24] HAADF-STEM was taken on C_s-corrected FEI Titan 80-300 FEG-S/TEM at the Pacific Northwest National Laboratory (PNNL).

Electrical resistivity and Hall measurements were determined using the van der Pauw technique[25] in the temperature range of 20−295 K. Samples were prepared on fused Quartz crystal slides in a 1 cm × 1 cm cross geometry. Further details on how temperature-dependent resistivity and Hall measurements were conducted are described elsewhere.[26]

RESULTS AND DISCUSSION

Table 1. Composition and Repeat Thickness of the AD Precursors and Annealed c-Lattice Parameters of a Selection of Precursors Prepared in This Study

sample	% Bi	% Se	% Ti	repeat thickness (Å)	c-axis lattice parameter (Å)
1	33.2(3)	57(1)	9.5(1)	26.8(1)	27.60(3)
2	30.8(3)	59(1)	10.0(1)	27.2(2)	27.5(1)
3	31.0(3)	59(1)	9.8(1)	29.1(2)	27.54(3)
4	29.3(3)	61(1)	9.3(1)	27.5(4)	27.4(2)
5	30.0(3)	61(1)	9.4(1)	29.2(4)	27.6(1)
6	30.8(3)	60(1)	9.4(1)	31.8(4)	27.5(2)
7	29.4(3)	62(1)	8.8(1)	32.0(5)	27.5(2)
8	31.0(3)	60(1)	9.4(1)	27.7(2)	27.67(4)

Table 1 summarizes the AD compositions determined from XRF measurements, repeat layer thicknesses, and c-axis lattice parameter of the heterostructure formed after annealing various precursors at 350 °C for 30 min for a representative suite of precursors prepared in this study. All of the precursors formed a compound with the expected c-axis lattice parameter after annealing, although the diffraction patterns indicated the presence of structural defects in most of the samples. The defects included extra diffraction maxima corresponding to Bi_2Se_3 in the Bi- and Se-rich precursors. Broadening of even order diffraction maxima was also observed in several of the samples. Broadening of specific 00l reflections occurs when an extra layer (perhaps $TiSe_2$ or Bi_2Se_3 in these samples) forms between regions that have crystalized the target heterostructure as the system self-assembles. The noninteger unit cell distance between the well-ordered regions results in an interference pattern between the two crystals.[14] Depending on the thickness of the intervening layer, different 00l reflections are broadened. The extent of broadening is related to the size of the two crystals and hence inversely related to the frequency of the extra layer. The extent of broadening indicates that the frequency of extra broadening is low. Within experimental error, the same heterostructures formed despite the variation in both composition and initial layer thickness of the precursor, suggesting that the targeted compound resides in a broad and relatively deep local free energy minimum in the free energy landscape.

To probe the formation of the targeted heterostructure and to determine the temperature range where it is stable, specular and in-plane XRD scans were collected after annealing sample 8 for 30 min at different temperatures (50 °C increments up to 450 °C). Surprisingly, there are resolvable Bragg reflections out to ∼65° 2θ in the AD sample, indicating that a coherent pattern of crystalline layers began to self-assemble during the deposition. The line widths of the broader reflections at higher angles (>10° 2θ) in the specular diffraction patterns, as shown in Figure 1, indicate a distribution of lattice spacings from an imperfect heterostructure. These reflections yield a c-axis lattice parameter of 27.67(4) Å. The sharp low-angle (<10° 2θ) reflections result from the compositional modulation of the precursor and yield a repeating thickness of the elemental modulation of 27.7(2) Å. As the annealing temperature is increased, the intensity of the higher angle reflections increases and the linewidths decrease, indicating that the layering is becoming more coherent. The low-angle reflections gradually shift to lower angles in the low-temperature regime, moving closer to the angles expected from the higher angle reflections. After annealing at 350 °C, all reflections can be indexed to a single family of reflections. This annealing temperature produces the highest intensities and narrowest line widths of the reflections without evidence of additional phases. We chose 350 °C as the optimal annealing temperature. The c-axis lattice parameter after the 350 °C annealing is 27.54(2) Å, which is

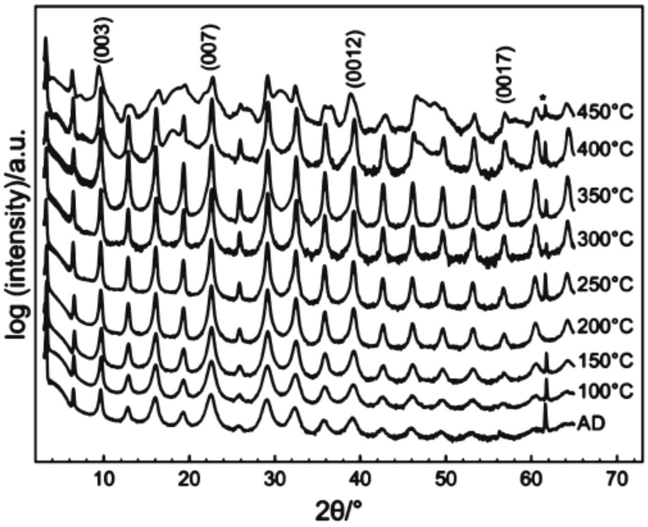

Figure 1. Specular diffraction patterns of a precursor annealed at the indicated temperatures for 30 min. The asterisk denotes Si reflections from the substrate.

slightly larger than the sum of the *c*-axis lattice parameters of the lattice parameters of Bi_2Se_3, $(BiSe)_{1.15}TiSe_2$[17] and the estimated thickness of an additional BiSe layer (27.05 Å).

After annealing the sample at 400 °C, additional reflections appear that are consistent with Bi_2Se_3 segregating from the superlattice. This is likely driven by the reaction of $TiSe_2$ with oxygen, which has previously been observed in metastable $[(BiSe)_{1+\delta}]_m[TiSe_2]_m$ compounds annealed at these temperatures.[13]

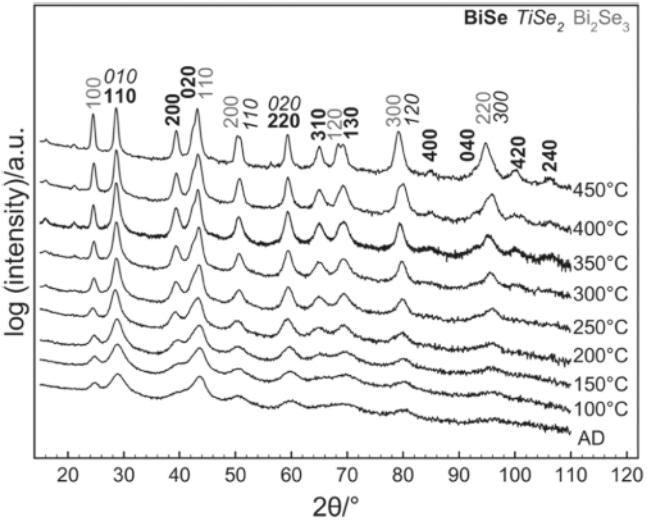

Figure 2. In-plane diffraction patterns of a precursor annealed at the indicated temperatures for 30 min.

In-plane diffraction data collected after each annealing step are shown in Figure 2. The AD precursor has Bragg reflections that indicate that the constituent layers nucleate and grow during the deposition process. The reflection at ∼25° 2*θ* can be indexed as the (100) reflection of Bi_2Se_3. Its presence indicates that the Bi_2Se_3 present in this sample has symmetry lower than that of bulk Bi_2Se_3. The reflection at ∼40° 2*θ* indicates that BiSe is also present. We do not know if $TiSe_2$ nucleates during deposition because the reflections for $TiSe_2$ overlap with those from Bi_2Se_3 and BiSe. As the annealing temperature is increased, the BiSe reflection at ∼40° 2*θ* becomes more defined and distinct from the reflection at ∼43° 2*θ* and the reflection at ∼68° 2*θ* splits into two reflections. This indicates that the BiSe layer(s) have a rectangular basal plane unit cell as has been reported previously.[17] After the 200 °C anneal, all reflections can be indexed to either BiSe, Bi_2Se_3, or $TiSe_2$, indicating that little or no additional phases are present. After the 250 °C anneal, two small reflections at ∼16° and ∼21° 2*θ* appear and grow in intensity as the annealing temperature increases. HAADF-STEM data, discussed next, suggest that these reflections result from periodic anti-phase boundaries in the BiSe layer. After the 450 °C anneal, the relative intensity of the Bi_2Se_3 reflections increases, which is consistent with specular diffraction data showing the presence of Bi_2Se_3 that is independent of the heterostructure. XRF measurements show an increase in the oxygen signal after annealing at 450 °C, which suggests that $TiSe_2$ is reacting with oxygen and the released Se reacts with BiSe to form Bi_2Se_3. This is consistent with reports of the complete conversion of thin layers of $TiSe_2$ to amorphous TiO_2 and elemental selenium under ambient conditions.[27] The in-plane lattice parameters from a full pattern Le Bail fit and *c*-lattice parameter are summarized in Table 2. The lattice parameters of $(BiSe)_{1.15}TiSe_2$ are provided for comparison.

Table 2. Lattice Parameters of $(BiSe)_{1+\delta}(Bi_2Se_3)_{1+\gamma}(BiSe)_{1+\delta}(TiSe_2)$ after the 350 °C Anneal[a]

lattice parameter	$(BiSe)_{1+\delta}(Bi_2Se_3)_{1+\gamma}-(BiSe)_{1+\delta}TiSe_2$	$(BiSe)_{1.15}TiSe_2$[17]
BiSe *a* (Å)	4.571(1)	4.562(2)
BiSe *b* (Å)	4.247(1)	4.242(1)
Bi_2Se_3 *a* (Å)	4.178(1)	
$TiSe_2$ *a* (Å)	3.596(1)	3.58(6)
$1 + \delta$	1.15	1.15
$1 + \gamma$	0.74	
c-axis (Å)	27.54(2)	11.776(6)

[a] Lattice parameters of $(BiSe)_{1.15}TiSe_2$[17] are provided for comparison.

To probe the local structure, HAADF-STEM images were collected. Figure 3 shows a HAADF-STEM image in which the top and bottom of the film are visible. The image confirms that the sample formed a periodic layered structure throughout the

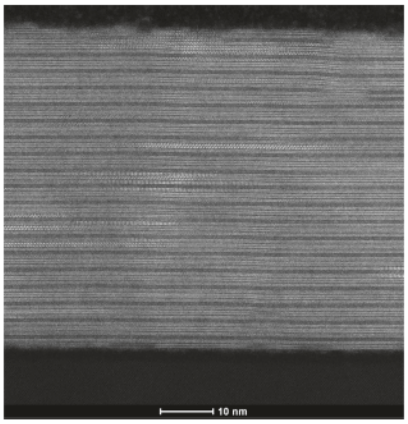

Figure 3. Medium magnification HAADF-STEM image of a representative precursor annealed at 350 °C for 30 min.

thickness of the film. The repeating unit contains one $TiSe_2$ trilayer, one Bi_2Se_3 quintuple-layer, and two BiSe bilayers separating the $TiSe_2$ and Bi_2Se_3 layers, which is consistent with the diffraction data. This stacking order may be due to an inherent instability in placing two or more BiSe bilayers next to one another or the BiSe layer may stabilize the structure by reducing the lattice mismatch between the $TiSe_2$ and Bi_2Se_3, as was hypothesized for $Bi_2Se_3/NbSe_2$ heterostructures.[28] No extended defects are present; however, a few quintuple layers of surface segregated Bi_2Se_3 are visible, suggesting that excess Bi and Se were present in the precursor or that the surface layer of $TiSe_2$ reacted with oxygen. Partial layers and other structural imperfections are visible at the top and bottom of the sample, presumably as a consequence of the self-assembly process.

In higher magnification HAADF-STEM images (Figure 4), all of the interfaces are atomically abrupt. The visible zone axis orientations change layer to layer, which is consistent with extensive turbostratic disorder. From images down the [100] zone axis of the $TiSe_2$ layers, we conclude that the Ti in $TiSe_2$ is octahedrally coordinated. When BiSe grains are orientated along a [110] zone axis, anti-phase boundaries are visible and appear regularly spaced. Similar anti-phase boundaries were previously seen in misfit layered compounds $(BiSe)_{1.10}NbSe_2$ and $(BiSe)_{1.09}TaSe_2$[29,30] and in rotationally disordered ferecrystalline compounds.[31−34] The Bi_2Se_3 layers contain the expected five-layer sequence of Se−Bi−Se−Bi−Se, and the orientation of these layers changes in a random manner throughout the sample. The structural coherency is significantly higher than what might be expected based on the ability to control the thickness and composition of each elemental layer in the deposition of the precursor. The high structural coherency indicates that atoms diffuse between layers during the self-assembly process.

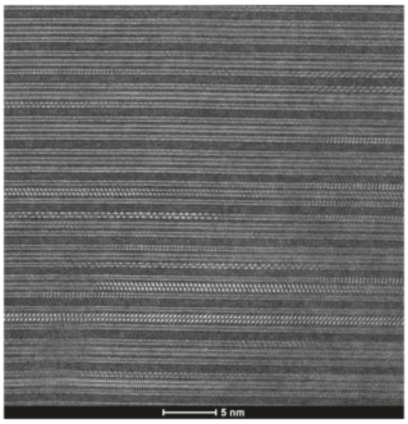

Figure 4. High magnification HAADF-STEM image of a representative precursor annealed at 350 °C for 30 min.

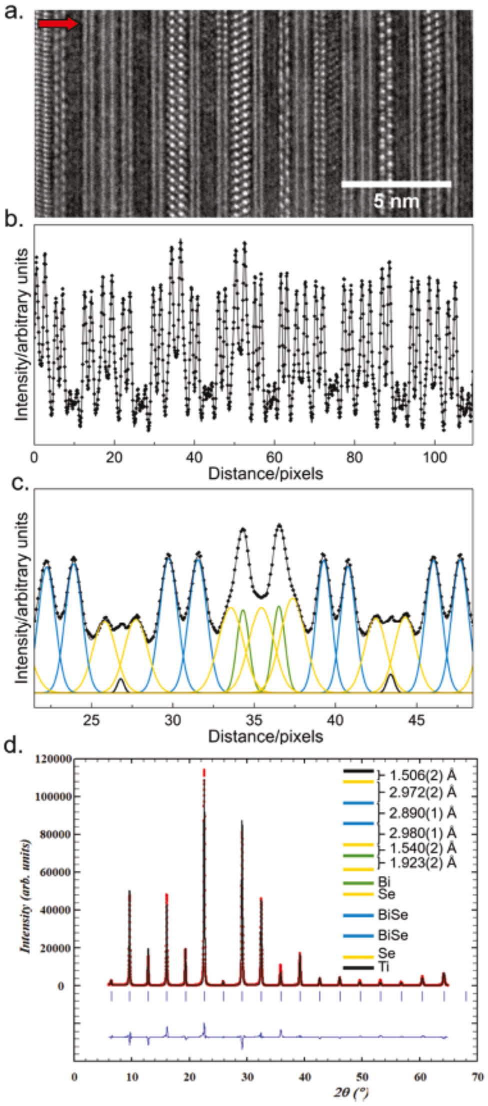

Figure 5. (a) High-resolution HAADF-STEM image showing atomic columns in several unit cells in $(BiSe)_{1+\delta}(Bi_2Se_3)_{1+\gamma}(BiSe)_{1+\delta}(TiSe_2)$, (b) intensity of the HAADF-STEM image integrated along the vertical direction and scanned in the direction of the arrow shown for the image in (a). The average integrated intensity of approximately one unit cell with fitted positions of individual Gaussian peaks for each atomic plane is shown in (c). The black peaks correspond to Ti planes, green to Bi, yellow to Se, and blue to BiSe. Rietveld refinement of the specular diffraction pattern is shown in (d) with the refined structural model shown as an inset on the right.

The atomic structure of the new compound was determined using a combination of HAADF-STEM and diffraction data. The positions of the atomic planes were determined by fitting the integrated HAADF-STEM intensity profiles to a sum of Gaussians. The positions determined from the HAADF-STEM image were used to create an initial model for Rietveld refinement of the specular diffraction. The region of the HAADF-STEM image used to create the initial model is shown in part (a) of Figure 5. The integrated HAADF-STEM intensity profile of this region, scanned in the direction indicated by the arrow, is shown in Figure 5b along with the fit to a sequence of Gaussian profiles. The Gaussian profiles used to fit the intensity profile of the averaged unit cell (c) are shown in Figure 5c. The green Gaussians correspond to Bi atoms, the yellow Gaussians to Se atoms, and the black Gaussians to Ti. It was not possible to spatially resolve the Bi and Se atomic planes in the BiSe layer, so they were fit as single Gaussians which are shown in blue. The Rietveld refinement of the specular diffraction (left) and the refined structural model (right) using the HAADF-STEM atomic plane positions as a starting model are shown in Figure 5d. The refined *c* axis-lattice parameter is 27.560(1) Å. In other compounds, the Bi and Se in BiSe layers pucker, where Bi moves outward toward the dichalcogenide and Se moves inward.[13,17] This puckering is not resolvable in $(BiSe)_{1+\delta}(Bi_2Se_3)_{1+\gamma}(BiSe)_{1+\delta}TiSe_2$. The separation of the Ti and Se atomic planes in the $TiSe_2$ layer is approximately 0.03 Å smaller than that found in bulk $TiSe_2$.[35] The separation of the planes in BiSe and the gap between $TiSe_2$ and BiSe are similar to those found in $(BiSe)_{1+\delta}[TiSe_2]_3$.[31]

To learn more about the in-plane structure of the BiSe planes, the HAADF-STEM images were integrated across the top and bottom of Bi–Se atomic planes that were orientated down what would be the rock-salt [110] zone axis (Figure 6a).

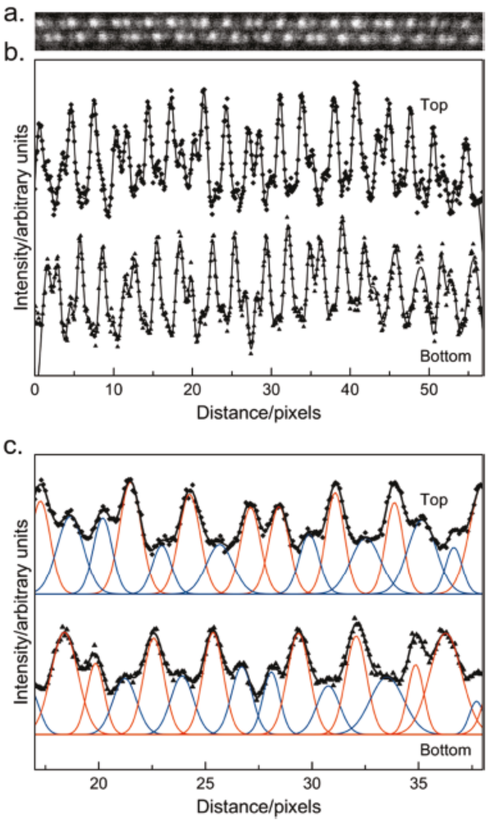

Figure 6. High-resolution cross-sectional HAADF-STEM image of the BiSe bilayer (a). The integrated intensity of the top atomic plane and the bottom atomic plane are shown in (b). The integrated intensity of the top plane and the bottom plane of one supercell with fitted positions of individual Gaussian peaks is shown in (c). The red peaks correspond to Bi atoms and blue to Se.

The intensity profile for the image is shown in Figure 6b. The average intensity profile was fit using the same procedure as described above for the atomic planes along the *z* axis. In the HAADF-STEM intensity profile shown in Figure 6c, the higher intensity peaks (red) correspond to Bi atoms and the remaining peaks correspond to Se atoms (blue). Most notable in the fit is the presence of periodic anti-phase boundaries. The anti-phase boundaries are spaced by five Bi–Se bonds. The Bi–Bi bonds on the top plane and bottom plane systematically alternate. These periodic anti-phase boundaries form a supercell that is similar to that reposted for the $(BiSe)_{1.09}TaSe_2$ misfit layer compound.[30] Different from the structure reported for $(BiSe)_{1.09}TaSe_2$ is a pronounced distortion that displaces some atoms in the top plane so that they are not directly atop the atoms in the bottom plane.

The displacement and the formation of a supercell explains the presence of forbidden reflections with respect to an undistorted rock salt structure in the in-plane diffraction pattern discussed earlier. An initial structural model for Rietveld refinement of the in-plane diffraction was constructed from the bulk structures of Bi_2Se_3 and $TiSe_2$ along with the BiSe structure obtained from the STEM image fit. Unfortunately, a satisfactory refinement could not be obtained because there are too many refinable parameters for the number of independent reflections. A full pattern Le Bail fit was used to refine the lattice parameters based on the expanded unit cell determined from the STEM images. The supercell enables indexing of the reflection at ~16° 2θ as the BiSe (500) reflection. The in-plane lattice parameters for Bi_2Se_3 (a = 4.178(1) Å) and $TiSe_2$ (a = 3.567(1) Å) are consistent with prior reports.[17,18,28] The in-plane lattice parameters for BiSe (a = 27.431(1) Å, b = 4.247(1) Å) are consistent with those previously reported for the misfit layered compounds $(BiSe)_{1.10}NbSe_2$ and $(BiSe)_{1.09}TaSe_2$.[29,30]

Temperature-dependent resistivity and Hall effect measurements collected between 20 and 295 K are shown in Figure 7. The resistivity for the new heterostructure is lower than that

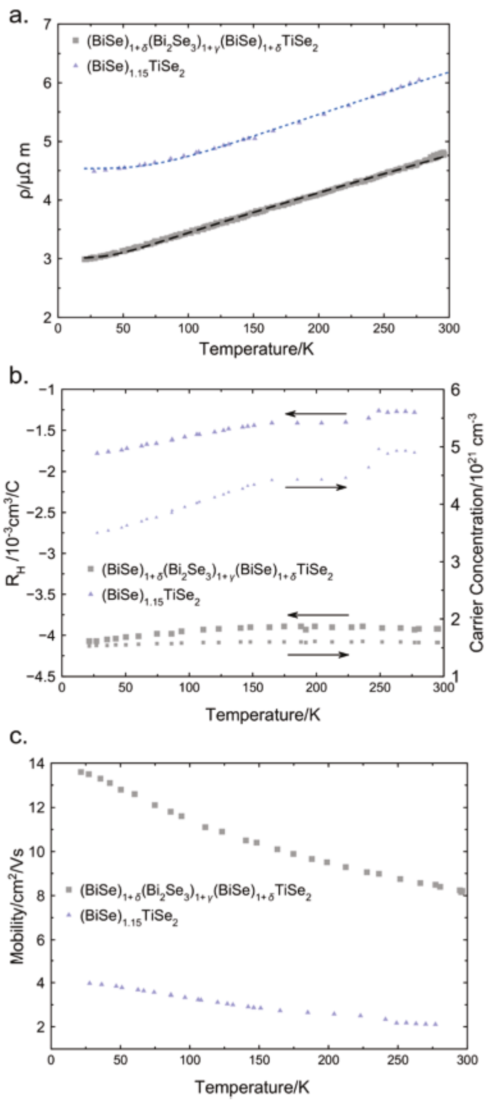

Figure 7. Temperature-dependent resistivity (a), Hall coefficient and carrier concentration (b), and carrier mobility (c) of $(BiSe)_{1+\delta}(Bi_2Se_3)_{1+\gamma}(BiSe)_{1+\delta}TiSe_2$ compared to $(BiSe)_{1.15}TiSe_2$.

reported for $(BiSe)_{1.15}TiSe_2$ at all temperatures and the temperature dependence indicates metallic behavior. Both compounds have lower resistivity than bulk $TiSe_2$, and neither compound shows evidence of the charge density wave that is seen in bulk $TiSe_2$.[36] A simple composite model would suggest that the addition of a semiconducting Bi_2Se_3 layer would increase the resistivity. To test if the average carrier concentration in the sample is increased by electron transfer from the additional BiSe layer relative to $(BiSe)_{1.15}TiSe_2$, the Hall coefficient was measured. The Hall coefficient is negative across the temperature range, indicating that electrons are the majority carrier type and nearly constant as a function of temperature as expected for a metal. Assuming a single band model, the larger magnitude of the Hall coefficient for the new heterostructure relative to $(BiSe)_{1.15}TiSe_2$ suggests that it has approximately half the carrier concentration. In $(BiSe)_{1.15}TiSe_2$, the change in carrier concentration relative to $(PbSe)TiSe_2$ suggests that BiSe donates electrons to $TiSe_2$.[17] Because Bi_2Se_3 is a semiconductor and there are two BiSe layers that can donate charge, one would expect the carrier concentrations to be about the same if this compound was approximated as a simple composite. This deviation from simple composite behavior suggests that interactions between the constituents are important. The mobility of the charge carriers was calculated from the resistivity and the Hall derived carrier concentration and is much higher in $(BiSe)_{1+\delta}(Bi_2Se_3)_{1+\gamma}(BiSe)_{1+\delta}TiSe_2$ than in $(BiSe)_{1.15}TiSe_2$. This suggests that the addition of a Bi_2Se_3 layer reduces the amount of scattering at the interfaces.

To gain a better understanding, the resistivity data were fit to the Bloch-Grüneisen model

$$\rho(T) = \rho_0 + \mathcal{R}\left(\frac{T}{\theta_D}\right)^5 \int_0^{\theta_D} \frac{z^5}{(e^z - 1)(1 - e^{-z})} dz$$

where ρ_0 is the residual resistivity, $\mathcal{R}$ is the electron−phonon interaction constant, and θ_D is the Debye temperature. The fitted parameters are reported in Table 3. The smaller ρ_0 indicates that the new heterostructure has a lower defect density than $(BiSe)_{1.15}TiSe_2$. The new heterostructure also has a substantially lower Debye temperature than $(BiSe)_{1.15}TiSe_2$. The decrease in the Debye temperature implies a change in the distribution of phonons in the material, which, given the structural changes in the BiSe layer and the addition of a Bi_2Se_3 layer, is perhaps expected.

Table 3. Bloch-Grüneisen Fit Parameters

parameter	$(BiSe)_{1+\delta}(Bi_2Se_3)_{1+\gamma}(BiSe)_{1+\delta}TiSe_2$	$(BiSe)_{1.15}TiSe_2$
P_0	3.016(5)	4.54(1)
$\mathcal{R}$	6.4(1)	12.4(5)
θ_D	262(6)	490(16)

The lower electron−phonon interaction constant of the $(BiSe)_{1+\delta}(Bi_2Se_3)_{1+\gamma}(BiSe)_{1+\delta}TiSe_2$ further indicates a change in the distribution of phonon modes as a function of energy. The lower ρ_0 for the new heterostructure might be a consequence of fewer defects; however, potential conduction through topologically protected states on the surface of the Bi_2Se_3 layers cannot be ruled out. The larger mobility and its increase with decreasing temperature suggests that there is less scattering from phonons, which is consistent with the decreased electron−phonon interaction constant. The properties of this new heterostructure cannot be modeled as a simple composite of the constituents. The layers interact with one another to produce emergent behavior. The single unit cell thickness of each constituent results in the environment of each layer being significantly different than that found in their respective bulk structures.

■ CONCLUSIONS

The synthesis of the title heterostructure presented herein suggests that many new metastable compounds could possibly be prepared via low-temperature synthesis approaches. Directing the synthesis toward a targeted compound is a major challenge in conventional synthesis approaches. The approach used in this paper, using a precursor with an architecture similar to that of the targeted kinetically stable heterostructure, can be adapted to a myriad of undiscovered compounds because the structure of the precursor can be varied to target specific intergrowths. Following changes in XRD patterns as a function of annealing temperature and time provides a sensitive probe of structural changes during the self-assembly. While the structures of the $TiSe_2$ and Bi_2Se_3 layers were similar to those found in the binary compounds and other intergrowth structures, the BiSe layers had a different structure than previous reports. The changes in the structure of the BiSe constituent relative to previously reported structures highlight the influence of neighboring layers. Electron transport measurements show an unexpected increase in carrier mobility and a decrease in carrier concentration compared to $(BiSe)_{1.15}TiSe_2$. These changes indicate that this new compound cannot be treated as a composite. Interlayer interactions result in both structural changes and emergent physical properties.

■ AUTHOR INFORMATION

Corresponding Author

*E-mail: davej@uoregon.edu.

ORCID

Alexander C. Lygo: 0000-0003-1762-244X
Suzannah R. Wood: 0000-0002-7208-7681
David C. Johnson: 0000-0002-1118-0997

Present Address

[†]XTD-IDA, Los Alamos National Laboratory, Los Alamos, New Mexico 87545, United States.

Author Contributions

The manuscript was written through contributions of all authors.

Notes

The authors declare no competing financial interest.

■ ACKNOWLEDGMENTS

Author A.C.L. acknowledges support from the University of Oregon Office of the Vice President of Research and Innovation (VPRI) and the Presidential Undergraduate Research Scholarship (PURS). The authors acknowledge support from the National Science Foundation under grant DMR-1710214. We would like to acknowledge the Center for Advanced Materials Characterization in Oregon (CAMCOR) at the University of Oregon for the equipment used in this investigation. We acknowledge support through the Collaborative Access Team (CAT): Pooled Resources for Electron Microscopy Informatics, Education and Research (PREMIER)

Network Program at Pacific Northwest National Laboratory (PNNL) and the Environmental Molecular Sciences Laboratory, a national scientific user facility sponsored by the DOE's Office of Biological and Environmental Research at PNNL. PNNL is operated by Battelle for the DOE under Contract DE-AC05-76RL01830. Los Alamos National Laboratory, an affirmative action/equal opportunity employer, is managed by Triad National Security, LCC, for the National Nuclear Security Administration of the U.S. Department of Energy under Contract 89233218CNA000001.

■ ABBREVIATIONS

XRF, X-ray fluorescence; XRD, X-ray diffraction; HAADF-STEM, high angle annular dark field scanning transmission electron microscopy; FEG-S/TEM, field-emission gun scanning-transmission electron microscope

■ REFERENCES

(1) Moore, J. E. The Birth of Topological Insulators. *Nature* **2010**, *464*, 194−198.

(2) Moore, J. Topological Insulators: The next Generation. *Nat. Phys.* **2009**, *5*, 378−380.

(3) Qi, X.-L.; Zhang, S.-C. Topological Insulators and Superconductors. *Rev. Mod. Phys.* **2011**, *83*, 1057−1110.

(4) Sato, M.; Ando, Y. Topological Superconductors: A Review. *Rep. Prog. Phys.* **2017**, *80*, 076501.

(5) Dang, W.; Peng, H.; Li, H.; Wang, P.; Liu, Z. Epitaxial Heterostructures of Ultrathin Topological Insulator Nanoplate and Graphene. *Nano Lett.* **2010**, *10*, 2870−2876.

(6) Zhang, Q.; Zhang, Z.; Zhu, Z.; Schwingenschlögl, U.; Cui, Y. Exotic Topological Insulator States and Topological Phase Transitions in Sb_2Se_3-Bi_2Se_3 Heterostructures. *ACS Nano* **2012**, *6*, 2345−2352.

(7) Hesjedal, T.; Chen, Y. Topological Insulators: Engineered Heterostructures. *Nat. Mater.* **2016**, *16*, 3−4.

(8) Zhang, H.; Liu, C.-X.; Qi, X.-L.; Dai, X.; Fang, Z.; Zhang, S.-C. Topological Insulators in Bi_2Se_3, Bi_2Te_3 and Sb_2Te_3 with a Single Dirac Cone on the Surface. *Nat. Phys.* **2009**, *5*, 438−442.

(9) Zhang, Y.; He, K.; Chang, C.-Z.; Song, C.-L.; Wang, L.-L.; Chen, X.; Jia, J.-F.; Fang, Z.; Dai, X.; Shan, W.-Y.; et al. Crossover of the Three-Dimensional Topological Insulator $Bi_2Se_3$to the Two-Dimensional Limit. *Nat. Phys.* **2010**, *6*, 584−588.

(10) Förster, T.; Krüger, P.; Rohlfing, M. Ab Initio Studies of Adatom- and Vacancy-Induced Band Bending in Bi_2Se_3. *Phys. Rev. B: Condens. Matter Mater. Phys.* **2015**, *91*, 035313.

(11) Valla, T.; Ji, H.; Schoop, L. M.; Weber, A. P.; Pan, Z.-H.; Sadowski, J. T.; Vescovo, E.; Fedorov, A. V.; Caruso, A. N.; Gibson, Q. D.; et al. Topological Semimetal in a Bi-Bi_2Se_3Infinitely Adaptive Superlattice Phase. *Phys. Rev. B: Condens. Matter Mater. Phys.* **2012**, *86*, No. 241101(R).

(12) Chen, P.; Zhang, Z.; Duan, X.; Duan, X. Chemical Synthesis of Two-Dimensional Atomic Crystals, Heterostructures and Superlattices. *Chem. Soc. Rev.* **2018**, *47*, 3129−3151.

(13) Lygo, A. C.; Hamann, D. M.; Moore, D. B.; Merrill, D. R.; Ditto, J.; Esters, M.; Orlowicz, J.; Wood, S. R.; Johnson, D. C. Kinetically Controlled Formation and Decomposition of Metastable $[(BiSe)_{1+\delta}]_m[TiSe_2]_m$ Compounds. *J. Am. Chem. Soc.* **2018**, *140*, 3385−3393.

(14) Beekman, M.; Rodriguez, G.; Atkins, R.; Kunert, J.; Moore, D. B.; Johnson, D. C. Detection of Nanoscale Embedded Layers Using Laboratory Specular X-Ray Diffraction. *J. Appl. Phys.* **2015**, *117*, 185306.

(15) Jansen, M.; Schön, J. C. "Design" in Chemical Synthesis—An Illusion? *Angew. Chem. Int. Ed.* **2006**, *45*, 3406−3412.

(16) Schön, J. C.; Jansen, M. First Step Towards Planning of Syntheses in Solid-State Chemistry: Determination of Promising Structure Candidates by Global Optimization. *Angew Chem. Int. Ed. Engl.* **1996**, *35*, 1286−1304.

(17) Merrill, D. R.; Moore, D. B.; Coffey, M. N.; Jansons, A. W.; Falmbigl, M.; Johnson, D. C. Synthesis and Characterization of Turbostratically Disordered $(BiSe)_{1.15}TiSe_2$. *Semicond. Sci. Technol.* **2014**, *29*, 064004.

(18) Lind, H.; Lidin, S. A General Structure Model for Bi-Se Phases Using a Superspace Formalism. *Solid State Sci.* **2003**, *5*, 47−57.

(19) Atkins, R.; Wilson, J.; Zschack, P.; Grosse, C.; Neumann, W.; Johnson, D. C. Synthesis of $[(SnSe)_{1.15}]_m(TaSe_2)_n$ Ferecrystals: Structurally Tunable Metallic Compounds. *Chem. Mater.* **2012**, *24*, 4594−4599.

(20) Le Bail, A.; Duroy, H.; Fourquet, J. L. Ab-Initio Structure Determination of $LiSbWO_6$ by X-Ray Powder Diffraction. *Mater. Res. Bull.* **1988**, *23*, 447−452.

(21) Rodríguez-Carvajal, J. Recent Advances in Magnetic Structure Determination by Neutron Powder Diffraction. *Phys. Rev. B: Condens. Matter Mater. Phys.* **1993**, *192*, 55−69.

(22) Roisnel, T.; Rodríquez-Carvajal, J. WinPLOTR: A Windows Tool for Powder Diffraction Pattern Analysis. *Mater. Sci. Forum* **2001**, *378−381*, 118−123.

(23) Hamann, D. M.; Bardgett, D.; Cordova, D. L. M.; Maynard, L. A.; Hadland, E. C.; Lygo, A. C.; Wood, S. R.; Esters, M.; Johnson, D. C. Sub-Monolayer Accuracy in Determining the Number of Atoms Per Unit Area in Ultrathin Films Using X-Ray Fluorescence. *Chem. Mater.* **2018**, *30*, 6209−6216.

(24) Schaffer, M.; Schaffer, B.; Ramasse, Q. Sample Preparation for Atomic-Resolution STEM at Low Voltages by FIB. *Ultramicroscopy* **2012**, *114*, 62−71.

(25) van der Pauw, L. J. A Method of Measuring Specific Resistivity and Hall Effect of Discs of Arbitrary Shape. *Philips Res. Rep.* **1958**, *13*, 1−9.

(26) Alemayehu, M. B.; Mitchson, G.; Ditto, J.; Hanken, B. E.; Asta, M.; Johnson, D. C. Charge Transfer between PbSe and NbSe 2 in $[(PbSe)_{1.14}]_m(NbSe_2)_1$ Ferecrystalline Compounds. *Chem. Mater.* **2014**, *26*, 1859−1866.

(27) Sun, L.; Chen, C.; Zhang, Q.; Sohrt, C.; Zhao, T.; Xu, G.; Wang, J.; Wang, D.; Rossnagel, K.; Gu, L.; et al. Suppression of the Charge Density Wave State in Two-Dimensional 1T-$TiSe_2$ by Atmospheric Oxidation. *Angew. Chem. Int. Ed.* **2017**, *56*, 8981−8985.

(28) Wang, M.-X.; Li, P.; Xu, J.-P.; Liu, Z.-L.; Ge, J.-F.; Wang, G.-Y.; Yang, X.; Xu, Z.-A.; Ji, S.-H.; Gao, C. L.; et al. Interface Structure of a Topological Insulator/Superconductor Heterostructure. *New J. Phys.* **2014**, *16*, 123043.

(29) Zhou, W. Y.; Meetsma, A.; de Boer, J. L.; Wiegers, G. A. Characterization and Electrical Transport Properties of the Misfit Layer Compounds $(BiSe)_{1.10}NbSe_2$ and (BiSe)1.09TaSe2. *Mater. Res. Bull.* **1992**, *27*, 563−572.

(30) Petříček, V.; Cisarova, I.; de Boer, J. L.; Zhou, W.; Meetsma, A.; Wiegers, G. A.; van Smaalen, S. The Modulated Structure of the Commensurate Misfit-layer Compound $(BiSe)_{1.09}TaSe_2$. *Acta Crystallogr., Sect. B: Struct. Sci.* **1993**, *49*, 258−266.

(31) Wood, S. R.; Merrill, D. R.; Falmbigl, M.; Moore, D. B.; Ditto, J.; Esters, M.; Johnson, D. C. Tuning Electrical Properties through Control of $TiSe_2$ Thickness in $(BiSe)_{1+\delta}(TiSe_2)_n$ Compounds. *Chem. Mater.* **2015**, *27*, 6067−6076.

(32) Wood, S. R.; Merrill, D. R.; Mitchson, G.; Lygo, A. C.; Bauers, S. R.; Hamann, D. M.; Sutherland, D. R.; Ditto, J.; Johnson, D. C. Modulation Doping in Metastable Heterostructures via Kinetically Controlled Substitution. *Chem. Mater.* **2016**, *29*, 773−779.

(33) Mitchson, G.; Falmbigl, M.; Ditto, J.; Johnson, D. C. Antiphase Boundaries in the Turbostratically Disordered Misfit Compound $(BiSe)_{1+\delta}NbSe_2$. *Inorg. Chem.* **2015**, *54*, 10309−10315.

(34) Mitchson, G.; Hadland, E.; Göhler, F.; Wanke, M.; Esters, M.; Ditto, J.; Bigwood, E.; Ta, K.; Hennig, R. G.; Seyller, T.; et al. Structural Changes in 2D BiSe Bilayers as n Increases in $(BiSe)_{1+\delta}(NbSe_2)_n$ (n = 1−4) Heterostructures. *ACS Nano* **2016**, *10*, 9489−9499.

(35) Riekel, C. Structure Refinement of $TiSe_2$ by Neutron Diffraction. *J. Solid State Chem.* 1976, *17*, 389−392.
(36) Di Salvo, F. J.; Moncton, D. E.; Waszczak, J. V. Electronic Properties and Superlattice Formation in the Semimetal $TiSe_2$. *Phys. Rev. B: Solid State* 1976, *14*, 4321−4328.